## 5.7 Maximal and submaximal exchange between two deep basins with rotation.

The exploration of two-layer hydraulic phenomena in rotating channels is quite limited in comparison to the nonrotating case. Progress to date has largely been limited to three special cases, the subjects of this and the following two sections. The first case is pure exchange flow over a sill separating two infinitely deep basins. The theory relies on the zero potential vorticity approximation in both layers, at least in the vicinity of the sill. The next section covers the case of the pure lock exchange through a contraction with no sill. By the nature of the initial value problem the potential vorticity in this case is uniform and finite. The third special case (Section 5.9) is the only one that involves a net barotropic flow. The novel feature is a scale mismatch between the baroclinic and barotropic components of the flow. The latter is confined to sidewall boundary layers while the former is felt all across the channel. Even in a wide channel the effects of forcing by one sidewall can be transmitted into the baroclinic boundary layer on the opposite wall through the barotropic flow. As this is written, very little is known regarding hydraulic jumps, bores, and other transient features of these flows. Very little is known regarding their stability. The following discussions of purely steady models only scratch the surface of what is undoubtedly a rich body of physical behavior.

We begin with what might seem to be a simple calculation-that of pure exchange over a sill between two deep basins. This problem, which is a natural extension of the Whitehead et al. (1974, Section 2.4) model for single-layer flow, turns out to be anything but simple. The same authors consider certain aspects of the two-layer problem and our discussion is based on their work as well as that of Dalziel (1988, 1990), Riemenschneider et al. (2005), and Timmermans and Pratt (2005).

Consider a rectangular channel that has uniform width and that separates two relatively wide and deep basins with horizontal bottoms. An exchange flow between the basins could be established as a result of a lock exchange experiment in which the basins are filled with fluids of densities $\rho_1$ and $\rho_2$ and are separated by a barrier that sits atop the sill (Figure 5.7.1a). If the barrier is removed the two layers can be expected to displace each other and flow into the opposite reservoirs. As usual, the basin that initially contains the denser fluid will be referred to as 'upstream' (Figure 5.7.1b) and the direction of its outflow will be considered positive. The layer depths in the initially quiescent reservoirs are the potential depths $D_{1\infty}$ and $D_{2\infty}$. The potential vorticity of the layers within the channel will therefore be $f/ D_{1\infty}$ and $f/ D_{2\infty}$, provided that the initially shallow water has been entirely washed out of the strait and that dissipation does not intervene. If the sill depth $D_s << D_{1\infty}$ and $<<D_{2\infty}$, then the definition (5.1.9) of semigeostrophic potential vorticity implies that

$$\left( f + \frac{\partial v_n{}^*}{\partial x^*} \right) / f = O\left( \frac{D_s}{D_{n\infty}} \right) << 1$$

in the vicinity of the sill. Therefore

$$\frac{\partial v_n{}^*}{\partial x^*} \cong -f \,, \tag{5.7.1}$$

as was the case in the single-layer analog.

As discussed in Chapter 2, models based on (5.7.1) are often referred to under the title *zero potential vorticity*. It is true that the relative vorticity exactly equals $-f$ when the potential vorticity of the flow is exactly zero. But (5.7.1) should in the present model be regarded as an approximation, valid only where the layer depth $d_n$* is small compared to its potential depth $D_{n\infty}$. The dimensional value of the potential vorticity need not be zero. Equation (5.7.1) and the derived relations (5.7.2-5.7.4) below can be expected to hold near the sill, but can fail as either of the deep reservoirs is approached. We will analyze the sill region first and return to the basin states later.

In terms of the nondimensional variables,

$$x = \frac{x^* f}{\sqrt{g' D_S}}, \quad y = \frac{y^*}{L}, \quad z = \frac{z^*}{D_S}, \quad v_n = \frac{v_n^*}{\sqrt{g' D_S}}, \text{ and } u_n = \frac{fL}{g' D_S} u_n^*,$$

the thermal wind relation (5.1.8) is

$$v_2 - v_1 = \frac{\partial d_2}{\partial x}, \tag{5.7.2}$$

while (5.7.1) becomes

$$\frac{\partial v_n}{\partial x} = -1 \,. \tag{5.7.3}$$

In addition, the dimensionless form of Crocco's relation (5.1.16) is $dB_n / d\psi_i = D_S / D_{n\infty}$. The Bernoulli functions $B_1$ and $B_2$ are therefore uniform where $D_S / D_{i\infty} << 1$, and it follows that the 'internal' Bernoulli function

$$\Delta B = B_2 - B_1 = \frac{1}{2}\left(v_2^2 - v_1^2\right) + d_2 + h \tag{5.7.4}$$

(see 5.1.17) is uniform wherever both layers are shallow with respect to their respective potential depths.

Equations (5.7.2) and (5.7.3) provide that the slope of the interface across the channel is constant. Some of the geometrically possible cross sections are shown in

Figure 5.7.2. *Attached flow* will refer to a state in which the layer depths remain finite across the channel (Frame *a* and *b*). For a lock exchange flow, the lower layer velocity will generally be positive and the upper layer velocity negative, so the interface will slope from left to right, as in Frame *a*. Other possible states are *singly detached* (Frames *c* and *c*) and *doubly detached* (Frame *d*). It will be convenient to redefine the location of the origin $x$=0 depending on the state of separation. The various cases of attachment and detachment are an artifact of the rectangular channel cross-section. Natural straits have a smoothly varying topography, but this introduces difficulties more serious than the bookkeeping required to keep track of the various modes of separation.

*a. Critical conditions at the sill.*

With the channel spanning $-w/2 < x < w/2$ the solutions to (5.7.2) and (5.7.3) can be written as

$$v_i(x,y) = -x + \overline{v}_n(y)\,, \tag{5.7.5}$$

$$d_1(x,y) = \left(d(y) - \overline{d}_2(y)\right) - \left(\overline{v}_2(y) - \overline{v}_1(y)\right)x\,, \tag{5.7.6}$$

and

$$d_2(x,y) = \overline{d}_2(y) + \left(\overline{v}_2(y) - \overline{v}_1(y)\right)x\,. \tag{5.7.7}$$

where $d = d_1 + d_2$ is the channel depth, $d$=1 at the sill, and the overbars denote the value of the quantity at the channel center, $x = 0$.

The volume fluxes $Q_n = Q_n^* f / g' D_S^2$ in layers $n$=1,2 can be calculated using (5.7.5)-(5.7.7) as

$$Q_1 = \int_{-w/2}^{w/2} v_1 d_1 dx = \overline{v}_1 \overline{d}_1 w + \left(\overline{v}_2 - \overline{v}_1\right)\frac{w^3}{12} \tag{5.7.8}$$

and

$$Q_2 = \int_{-w/2}^{w/2} v_2 d_2 dx = \overline{v}_2 \overline{d}_2 w - \left(\overline{v}_2 - \overline{v}_1\right)\frac{w^3}{12}\,. \tag{5.7.9}$$

The dimensional versions are given by

$$Q_{1,2}^* = \overline{v}_{1,2}^* \overline{d}_{1,2}^* w^* \pm \left(\overline{v}_2^* - \overline{v}_1^*\right)\frac{w^{*3} f^2}{12 g'} \tag{5.7.10}$$

In the absence of rotation, the first term on the right would give the layer transport. With rotation the velocity in each layer decreases as *x* increases. If $\overline{v}_2 - \overline{v}_1 > 0$, the interface slope is positive and the lower layer is thicker on the right-hand side of the channel (facing in positive *y* direction). This thicker portion has smaller (perhaps even negative) velocities compared to the velocities in the thinner left-hand side. Hence the positive interface tilt reduces the transport in the lower layer. A similar effect occurs in the upper layer and thus rotation reduces the net exchange $Q_2 - Q_1$ relative to the value based on the average layer velocity and depth. This trend is reminiscent of the tendency of rotation to reduce transports in single-layer overflows. It will be shown later, however, that the tendency is reversed, at least in theory, when the two-layer flow becomes doubly detached from the sidewalls.

Attention is now restricted to pure exchange flow

$$Q = -Q_1 = Q_2 > 0\,. \tag{5.7.11}$$

Use of this relation with (5.7.8) and (5.7.9) leads to

$$\overline{v}_1 \overline{d}_1 = \overline{v}_1 \left( d - \overline{d}_2 \right) = -\overline{v}_2 \overline{d}_2 \tag{5.7.12}$$

and it follows from (5.7.8) that

$$\overline{v}_2 = \frac{\left( Q / w \right)\left( d - \overline{d}_2 \right)}{\overline{d}_2 \left( d - \overline{d}_2 \right) - w^2 d / 12} \tag{5.7.13}$$

and

$$\overline{v}_1 = \frac{-\left( Q / w \right)\overline{d}_2}{\overline{d}_2 \left( d - \overline{d}_2 \right) - w^2 d / 12}\,. \tag{5.7.14}$$

A function $\mathcal{G}$ relating a the single variable $\overline{d}_2$ to the geometric parameters can be found by substituting the last two relations for the velocities in (5.7.4):

$$\mathcal{G}\left( \overline{d}_2 ; d, w \right) = \frac{Q^2 d \left( d - 2\overline{d}_2 \right)}{2w^2 (\overline{d}_2 (d - \overline{d}_2) - w^2 d / 12)^2} + \overline{d}_2 + h - \Delta B = 0 \tag{5.7.15}.$$

Application of the critical condition $\partial \mathcal{G} / \partial \overline{d}_2$ leads to

$$\frac{Q^2}{w^2} = \frac{\left(\bar{d}_2\left(d-\bar{d}_2\right) - w^2 d/12\right)^3}{d\left(\bar{d}_2\left(d-\bar{d}_2\right) - w^2 d/12 + \left(d-2\bar{d}_2\right)^2\right)}\ , \qquad (5.7.16)$$

which can also be written as

$$\frac{\bar{v}_1^2\bar{d}_2 + \bar{v}_2^2\bar{d}_1 - w^2\left(\bar{v}_2-\bar{v}_1\right)^2/12}{\left(\bar{d}_1\bar{d}_2 - w^2 d/12\right)} = 1\,. \qquad (5.7.17a).$$

The left side of (5.7.17) can be viewed as the square of a composite Froude number that characterizes the hydraulic state as subcritical, critical or supercritical for values <1, =1 or >1. In dimensional terms, the composite Froude number is given by

$$G_r^{\ 2} = \frac{\bar{v}_1{}^{*2}\,\bar{d}_2{}^* + \bar{v}_2{}^{*2}\,\bar{d}_1{}^* - \dfrac{w^{*2}\,f^2}{12g'}\left(\bar{v}_2{}^* - \bar{v}_1{}^*\right)^2}{g'\left(\bar{d}_1{}^*\,\bar{d}_2{}^* - \dfrac{w^{*2}\,f^2}{12g'}d^*\right)}\,. \qquad (5.7.17b)$$

In the limit of weak rotation $\left(w^{*2}\,f^2/g'd_n{}^* \to 0\right)$ it reduces to the familiar $G^2 = \dfrac{\bar{v}_1^2}{\bar{d}_1} + \dfrac{\bar{v}_2^2}{\bar{d}_2} = \dfrac{\bar{v}_1{}^{*2}}{g'\bar{d}_1} + \dfrac{\bar{v}_2{}^{*2}}{g'\bar{d}_2}$ for nonrotating flow. The symmetric state of marginal separation, where the interface contacts the upper right and lower left corners of the channel, is a possible critical state and can be shown to occur when $d=w^2$ (or $w^*=(g'd^*)^{1/2}/f$ (see exercise 4).

It can be shown (Exercise 5) that the characteristic speeds for the two-layer system under conditions of attachment, and allowing for net barotropic flow, are given by

$$c_\pm = \frac{\bar{v}_2\bar{d}_1 + \bar{v}_1\bar{d}_2}{d} \pm \left(1 - \frac{(\bar{v}_2-\bar{v}_1)^2}{d}\right)^{1/2}\left(\frac{\bar{d}_1\bar{d}_2}{d} - \frac{w^2}{12}\right)^{1/2}\,. \qquad (5.7.18)$$

Aside from the factor of $w^2/12$, this formula is identical to its nonrotating counterpart (5.2.1). The critical condition (5.7.17) can be obtained by setting $c_-=0$ and using $\bar{v}_1\bar{d}_1 + \bar{v}_2\bar{d}_2 = 0$.

The regularity condition (1.5.4) can be applied to (5.7.15) to determine further restrictions on the location of a section of hydraulic control. Attention is confined to the channel portion of the domain, for which $w$ = constant. After use of (5.7.16) and some lengthy algebra, the condition reduces to

$$\left[\left(d-\bar{d}_2\right)^2-\frac{w^2 d}{12}\right]\frac{dh}{dy}=0 \qquad (5.7.19)$$

The control section can lie where $dh/dy = 0$ (as at the sill) or at a virtual control $(\bar{d}_2=\bar{d}_{2v})$, where

$$\bar{d}_{2v}=d-\frac{wd^{1/2}}{2\sqrt{3}}. \qquad (5.7.20)$$

In the limit of weak rotation ($w\to 0$), satisfaction of (5.7.19) requires $\bar{d}_{2v}\to d$. The virtual control in this case occurs in the deep reservoir, when the upper layer is thin and the lower layer is infinitely deep and inactive. Rotation allows the virtual control to occur in the shallow reaches of the channel.

For attached flow, the volume flux for a particular critical sill state is obtained by setting $d$=1 in (5.7.16). The flux depends on the mean lower layer thickness $\bar{d}_2=\bar{d}_{2c}$ and the channel width $w$ (Figure 5.7.3.). In order to ascertain the effect of rotation on the flux, it is best to plot the flux per unit width $Q/w$ $\left(=Q^*/\left(w^* g'^{1/2} D_s^{3/2}\right)\right.$ since $f$ does not appear in the scaling for this quantity. For fixed $\bar{d}_{2c}$, the transport per unit width is reduced as the strength of rotation ( $w=w^* f/\sqrt{g'D_s}$ ) is increased. The gaps in the $w$ = 0.87 curve correspond to $\bar{d}_2$ values over which the flow becomes detached from one of the sidewalls. For $w \le 0.866$, the flow at the sill is always attached to both sidewalls; for

According to Figure 5.7.3, the maximum possible $Q/w$ for any $w$ occurs when $\bar{d}_{2c}$ = 1/2. The corresponding critical states are symmetrical in that the interface passes through mid-depth at the channel center ($x$=0) and the cross-sectional areas occupied by the two layers are identical. According to (5.7.16) the flux is given by

$$Q/w=\frac{1}{4}\left(1-\frac{w^2}{3}\right) \qquad (5.7.21)$$

or $Q^*=\dfrac{w^* g'^{1/2} D^{3/2}}{4}\left[1-\dfrac{w^{*2} f^2}{3g'D}\right]$. In the limit of weak rotation ($w\to 0$), $Q$ reduces to its maximal value $w/4$ for lock exchange through a pure contraction. The opposite extreme

occurs when the channel is sufficiently wide to cause separation, which first occurs when the interface strikes the upper right and lower left corners. The reader may wish to verify that this marginal state requires $d=w^2$, or $w^*=(g'd^*)^{1/2}/f$ (see Exercise 4). Since $d=1$ at the sill, double separation of the critical flow occurs when $w=1$, implying

$$Q = \frac{1}{6}, \tag{5.7.22}$$

or $Q^* = \frac{1}{6}\frac{g'D^2}{f}$.

In an analysis that assumes symmetry between layers, Whitehead et al. (1974) derived this and the former expression. They also speculated that (5.7.22) would continue to hold after the flow becomes detached from both sidewalls. The basic notion is that the detached flow, which would resemble that of Frame *e* of Figure 5.7.2, would be quiescent in the flange regions occupied by only one of the layers. This idea is inconsistent with the maintenance of zero potential vorticity throughout each layer. Also, as we will eventually see, symmetrical critical states at the sill cannot be smoothly connected to deep upstream basin. As in the nonrotating case, the lower layer is relatively thin at the sill and the flux is less than that given above. The flow in inherently asymmetrical due to the fact that the topography contacts only the lower layer. The maximum attainable exchange flux is therefore less than for $\overline{d}_{2c} = 1/2$. Symmetrical states would appear to be appropriate for a lock exchange flow carried out in the pure contraction. One difficulty with this scenerio is that the vortex squashing mechanism responsible for generating 'zero' potential vorticity would be lacking. It is therefore difficult to justify the corresponding flux formula, including the '1/6th' law, by any dynamically consistent argument. Despite these difficulties (5.7.21,22) have been shown to be relevant, either as a bound on, or an approximation of, laboratory exchange through a contraction. This matter will be discussed in Section 5.8.

The interface may detach from one or both of the sidewalls in a variety of ways. The three possibilities relevant to the lock exchange experiment are shown by the lower panels in Figure 5.7.2. An analysis of the type just described can be performed for each case, though the algebra is a bit more involved. A case with single separation is worked through in Exercise 3 and the case of double separation (Figure 5.7.2d) can be found in Timmermans and Pratt (2005). The results can be used to extend Figure 5.7.3 to cases of separated sill flow (Figure 5.7.4), in which $Q/w$ is plotted as a function of the separated width: $w_s$ for single separation and $w_b$ for double separation. For example, associated with the sill width $w=2.0$ is a range of critical solutions beginning with a singly separated case of zero width ($w_s=0$) and zero flux. As $w_s/w$ is increased the flux increases and double separation occurs at $w_s/w \cong .34$. Beyond this point the (dashed) curve for singly attached flow becomes solid, signifying double separation. The horizontal axis must now be interpreted as $w_b/w$ (Figure 5.7.2d). For narrow channel widths (specifically $w<1.01$) double separation does not occur. By symmetry, $w_s$ may be interpreted in Figure 5.7.4 as

the lower layer width for lower layer detachment or the upper layer width for upper layer detachment.

The curves in Figure 5.7.4 suggest, not surprisingly, that double separation occurs more readily as $w$ increases. In addition, the maximum possible $Q/w$ increases as rotation increases. It will be shown later that the maximal $Q/w$ that can be linked to a deep upstream basin (indicated by stars in the figure) actually decreases with increasing $w$ for singly separated flows. However this trend is reversed when double separation occurs. Another subtlety is that the relationship between $Q$ and $w_s$ is not always unique for a given $w$. There are two sets of curves for $0.866 \le w \ge 1.720$, as represented in the Figure by $w$= 0.87, 1.0, and 1.5. The second set of curves appear in the lower right of Figure 5.7.4 and is associated with relatively small values of $Q/w$. The significance of these solutions is not well understood.

*b. The Froude number plane.*

Attention has thus far been confined to the sill, where the flow is assumed to be critical. In order to extend the solution upstream and downstream, and thereby describe the solution for the channel as a whole, one can use conservation of layer fluxes and internal energy. In the absence of background rotation, the solutions are conveniently represented in the layer Froude number plane (e.g. Figure 5.3.1a). As shown by Reimenschneider et al. (2005), a similar approach is possible here, though under more restricted circumstances.

The governing relationships for the case of attached flow can be derived by using (5.7.11) to write the lower layer transport relation (5.7.9) and the Bernoulli equation (5.7.4) in the forms

$$Q_2 = Q = \frac{\overline{v}_2 \overline{v}_1 w d}{(\overline{v}_1 - \overline{v}_2)} + (\overline{v}_2 - \overline{v}_1)\frac{w^3}{12}$$

and

$$\Delta B - z_T = \frac{\overline{v}_1^2 - \overline{v}_2^2}{2} + \frac{\overline{v}_1 d}{\overline{v}_1 - \overline{v}_2} - d\,.$$

Division of these two by factors of $d^2$ and $d$ respectively, leads to

$$\frac{Q}{d^2} = \frac{\overline{F}_1 \overline{F}_2}{\overline{F}_1 + \overline{F}_2}\left(\frac{w}{d^{1/2}}\right) - \frac{\overline{F}_1 + \overline{F}_2}{12}\left(\frac{w}{d^{1/2}}\right)^3 \qquad (5.7.23)$$

and

$$\frac{\Delta B - z_T}{d} = \frac{\overline{F}_2^2 - \overline{F}_1^2}{2} - \frac{\overline{F}_2}{\overline{F}_1 + \overline{F}_2}\,, \qquad (5.7.24)$$

where

$$\bar{F}_n = \frac{\bar{v}_n}{d^{1/2}} = \frac{\bar{v}_n^*}{(g'd^*)^{1/2}} . \qquad (5.7.25)$$

$\bar{F}_1$, $\bar{F}_2$ are pseudo Froude numbers based on the total depth and layer velocities at mid-channel.

In the Froude number plane representation for nonrotating flow, a form of the energy equation (e.g. 5.3.1 or 5.4.1) was used to construct solution curves in the space of the layer Froude numbers $F_1$ and $F_2$. For a given range of bottom elevation or channel width, one traces out a solution by moving along the appropriate constant-energy curve. Control points occur where the solution curve intersects the critical diagonal $F_1^2+F_2^2=1$. The range of bottom elevation (or width) is specified by contours that cross the energy curves and are based on the continuity equation (5.2.9). A similar construction in terms of the pseudo Froude numbers $\bar{F}_1$, $\bar{F}_2$ is possible, but there are several complicating factors. One is that that the energy $(\Delta B - z_T)$ depends not only on $\bar{F}_1$ and $\bar{F}_2$ but also $d$. A more suitable quantity on which to base solution contours is $Q^{1/2} / (\Delta B - z_T)$, which depends on $\bar{F}_1$, $\bar{F}_2$ and on the ratio of the channel width to the 'local' radius of deformation:

$$\frac{w}{d^{1/2}} = \frac{w^*}{(g'd^*)^{1/2}} .$$

If the topography is chosen such that this ratio remains constant, then $Q^{1/2} / (\Delta B - z_T)$ depends only on the Froude numbers and contours of this function represent solutions in the Froude number plane (Figure 5.7.5). The channel geometry must therefore be one in which width varies in proportion to the square root of depth.

A second complication with the Froude number plane is in the representation of various regions with flow separation (Figure 5.7.5 inset). Where single or double detachment occurs the governing equations must be reformulated. It can be shown that $Q^{1/2} / (\Delta B - z_T)$ continues to depend only on $\bar{F}_1$, $\bar{F}_2$ and $w/d^{1/2}$. The corresponding solution curves can therefore be extended and are shown in the main part of the figure. $\bar{F}_1$ and $\bar{F}_2$ continue to be defined in terms of the velocities at $x$=0. In cases of extreme separation, the upper (or lower) layer may not exist at midchannel and the corresponding $\bar{v}_1$ (or $\bar{v}_2$) will cease to be physically meaningful. In such cases, $\bar{F}_1$ (or $\bar{F}_2$) is defined by extrapolation to ($x$=0) using the mathematical form of $v_1$ (or $v_2$) valid in the non-separated region. Although the Froude numbers so defined may have little physical meaning, they continue to act as a formal representation of the flow state.

In order to trace solutions along such curves for a given range in $d$, contours of constant $Q/d^2$ can be plotted. Equation (5.7.23) can be used for this purpose in the attached region, while modified relations hold in the other regions. The resulting contours are shown as dashed curves in Figure 5.7.5. For the case shown, the value of $d$ is infinite at the origin, corresponding to a deep upstream (or downstream) reservoir. If $Q$ is regarded as fixed, then shallower depths are found by moving away from the origin.

We may regard $Q^{1/2}/(\Delta B - z_T)$ and $Q$ as Gill-type functions that depend on $\bar{F}_1$ and $\bar{F}_2$ as well as the geometric variables $d$ and $w/d^{1/2}$. Critical flows therefore occur where

$$J_{\bar{F}_1,\bar{F}_2}[Q^{1/2}/(\Delta B - z_T), Q/d^2] = 0 .$$

There are two geometrically distinct situations where this condition is satisfied. The first (indicated by stars in Figure 5.7.5) lie where the (solid) solution curves and (dashed) topographic curves make grazing contact. These correspond to sill controls. The second (indicated by a single square) occurs where two solution curves cross. The Jacobian vanishes here because $Q^{1/2}/(\Delta B - z_T)$ is locally constant. Since the bottom elevation changes as one follows a solution curve through the intersection point, this point is a virtual control.

The overall geometry of the cases shown in Figure 5.7.5 is similar in some respects to the Froude number planes for nonrotating flow through a contraction, particularly Figure 5.4.1a. However there are also some important differences. To start with, there is nothing so simple as the critical diagonal; critical flows now occur along the arc indicated by a heavy dashed line in the inset. Flow states lying below this curve are subcritical. Also, where there was a single family of submaximal solutions with sill controls, there are now two. The first begins in the subcritical region at a point lying along the $\bar{F}_1$ axis and ends at a point on the $\bar{F}_2$ axis. The second begins at the former point and ends at another point on the $\bar{F}_1$ -axis. Each member of this second family passes through a sill control.

Of the submaximal solutions, the ones beginning on the $\bar{F}_1$ -axis and ending on the $\bar{F}_2$ axis are most consistent with physical expectations. An example corresponding to the -1.4-contour appears in Figure 5.7.6. At the upstream end, which corresponds to the left ends of the panels, the flow is subcritical, the lower layer is very deep and the upper layer is separated (panel *a*). The lower layer mid-channel velocity $\bar{v}_2$ is nearly zero and bands of positive and negative flow exist on the left and right walls (panel *b*). As the channel narrows and shoals the flow becomes attached and the lower layer velocity becomes unidirectional. As the sill is passed, the lower layer separates and becomes strongly trapped to the right wall. The upper layer becomes very deep and develops the same swirl velocity with backflow that characterized the upstream lower layer (panel *c*). The

second group of submaximal solutions has deep lower layers at both ends of the channel and does appear as relevant to the lock exchange problem. These solutions correspond to the set of small-flux solutions that appear in the lower right corner of Figure 5.7.4.

There is also a single solution with properties vaguely similar to the nonrotating maximal solution for flow through a pure contraction (curve *jbk* of Figure 5.4.1b). The corresponding solution curve begins In Figure 5.7.5 along the $\bar{F}_1$ -axis near $\bar{F}_1$ =0.5 and continues through a virtual control (square), becoming subcritical and then passing through a sill control (star) and ending on the $\bar{F}_2$ -axis. The later termination coincides with the downstream termination of the previously discussed submaximal solutions. There the lower layer is thin, separated and unidirectional, while the upper layer is deep and has bidirectional flow. It can also be shown that the upstream state, which lies near $\bar{F}_1$ =0.5 and $\bar{F}_2 = 0$, has a relatively deep, swirling lower layer and a separated and unidirectional upper layer. Both end states would almost certainly terminate in hydraulic jumps before the basin depth became infinite. The maximal nature of the flux for this solution is confirmed by the fact that the dashed contour lying at the sill control indicates a flux than is larger than for the previously considered solutions.

It is possible to construct other solutions that are more difficult to connect to deep upstream basins. For example the solution curve that begins along the $\bar{F}_1$ axis near $\bar{F}_1$ =0.2 and passes through the virtual control, is similar to the curve *abc* of Figure 5.4.1b, which was disqualified under conditions of exchange flow for reasons of long-wave instability. However, the general level of numerical and laboratory verification of any of the solutions is poor. We also note that unlike the previous Froude number plane representation, in which the direction of the velocity in any particular layer is arbitrary, the present solution curves apply only to exchange flow.

*c. Connecting the sill flow to the upstream basin.*

The solutions represented in the Froude number plane predict that strong recirculations will develop within at least one of the layers as the upstream or downstream basin is approached. This property derives from the global enforcement of the 'zero potential vorticity' condition $\partial v_n^* / \partial x^* = -f$. While this condition will hold near the sill, or wherever else the layer thickness is much less than its potential depth $D_{n\infty}$, it becomes untrustworthy where the layer thickness becomes as large as $D_{n\infty}$. In the initial value experiment suggested in Figure 5.7.1a, $D_{n\infty}$ is just the initial depth of layer *n* in the basin of origin. After the exchange flow has been initiated, the upstream depth of either layer can be expected to decrease a relatively small amount, and vorticity thus generated should also be small compared with *f*. In other words the layers are expected to remain relatively quiescent in their basins of origin.

Let us now consider a model that incorporates this view and thereby acts as an alternative to the model with global zero potential vorticity. For simplicity, assume that the width $w$ of the strait separating the two basins is constant and that all changes in total depth $D$ occur within the strait (Figure 5.7.1b). The upstream basin formally begins at the channel *mouth*, where the channel starts to widen. We denote the width in this widening region $w_B(y)$ and note that the depth $D$ there is already very large in comparison to $D_s$. The upper layer in this basin is expected to be relatively shallow and therefore subject to the zero potential vorticity approximations. The corresponding velocity and depth profiles are therefore determined by the single-layer expressions for zero potential vorticity: (2.2.29,30) for attached flow or (2.3.11,12) for separated flow. In the present context it is convenient to rewrite the expressions for attached flow as

$$v_1(x) = \frac{2\hat{d}(y)}{w_B} - x \tag{5.7.26}$$

$$d_1(x,y) = \bar{d}(y) + \frac{2\hat{d}(y)}{w_B(y)} - x \tag{5.7.27}$$

where $\bar{d}$ and $\hat{d}$ are one half the sum and difference of the depths at the side walls $x=\pm w_B/2$ (see 2.2.5 and 2.2.6). The associated flux and internal Bernoulli functions are given by

$$Q = -2\hat{d}\bar{d} \tag{5.7.28}$$

and

$$\Delta B = -\frac{2\hat{d}^2}{{w_B}^2} - \frac{{w_B}^2}{8} - \bar{d} + z_T \tag{5.7.29}$$

where $v_o$ and $d_o$ are the velocity and depth at the side wall, here $x=-w_b/2$.

If the upper layer is detached, it is convenient to redefine $x=0$ as lying at the left wall. The corresponding profiles are given by

$$v(x,y) = v_o(y) - x \tag{5.7.30}$$

and

$$d(x,y) = v_o(y)x - \frac{x^2}{2} + d_o(y)\,, \tag{5.7.31}$$

where $v_o$ and $d_o$ are the left wall velocity and depth. The flux and Bernoulli function for this case are given by

$$Q = d_o^2 / 2 \tag{5.7.32}$$

and

$$\Delta B = -\frac{v_o^2}{2} + z_T - d_o\,, \tag{5.7.33}$$

and the latter is obtained by evaluating (5.7.4) at the left wall. The separated current width $w_e$ can be related to $Q$ by

$$v_o = \frac{w_e}{2} - \frac{d_o}{w_e} = \frac{w_e}{2} - \frac{(2Q)^{1/2}}{w_e}\,, \tag{5.7.34}$$

which follows from setting $d$=0 at $x$=$w_e$.

At this stage we have written down expressions for the upper layer velocity and depth that are valid in the vicinity of the mouth and points upstream. The derivation is based on the hypothesis that the lower layer is deep and quiescent and the upper layer is thin. In order to smoothly connect the flow at the mouth ($w$=$w_B$) to one of the previously described critical sill states, for which both layers are active, we require that the two states have equal values of $\Delta B$ and $Q$. Since the mouth flow may be attached or detached, and the sill flow may lie in one of four configurations, a good deal of bookkeeping is required to check through all the possibilities. The general procedure is to begin with one of the critical sill flows represented in Figure 5.7.3 or 4, then check whether there is a mouth state, either attached or detached, with the same $\Delta B$ and $Q$. Proceeding thus will lead to one of three possibilities. First, there are no mouth states and therefore no smooth connection to the upstream basin. Examples are the fore mentioned sill flows that lie at the maxima of the Figure 5.7.3 curves. The second possibility is that there are two mouth states, one subcritical and one supercritical. In this case, prior experience suggests selection of the subcritical root as the appropriate upstream state. The resulting solution can be considered submaximal. Finally, there exists a single, hydraulically critical, mouth state. The solution associated with the final possibility will have maximal flux and will have two controls, one at the mouth and one at the sill.

As an example, consider the case $w$=0.5. The possible critical sill states are all attached and are specified along the middle curve in Figure 5.7.3. Begin at the lower left extremity of the curve, where both $\bar{d}_c$ and $Q/w$ are small. For each location on this portion of the curve there are two possible mouth states, one supercritical and one subcritical. As one proceeds to the right, the value of $Q/w$ increases and the two mouth states converge, eventually merging to a critical state. This state, which is indicated by a cross in the figure, is the maximal state for the $w$ in question. For higher values of $\bar{d}_c$ there are no physically meaningful mouth states, and thus the whole right-hand portion of the diagram is irrelevant to the problem at hand. The maximal $Q/w$ for each case is always less than maximum the value of the curve in question.

An interesting point of departure from the solutions with globally zero potential vorticity is in the location of upstream control. For the solutions under discussion, the upstream control lies at the mouth of the strait. For the Froude number plane solutions based on the global enforcement of zero potential vorticity, the upstream (virtual) control lies within the strait (see 5.7.20). Both results must answer to criticism; in the first case the upstream control is imposed by hypothesis, in the second the control may lie where the zero potential vorticity approximation fails. However, it turns out that the maximal fluxes predicted in either case differ by a negligible amount. The dots on the curves of Figure 5.7.3 indicate the maximal flow rate obtained when the zero potential vorticity relations are enforced globally. They indicate $Q/w$ values that lie only slightly above the maximal fluxes obtained with a mouth control. Moreover, no virtual controls within the channel are found once the sill flow becomes separated.

A similar set of calculations can be carried out for separated sill flows. An overall view of the maximal solutions thus obtained for various $w$ appears in Figure 5.7.7. It can be shown that the maximal $Q/w$ for a given $w$ is always less than the maximum value permitted by the critical condition alone. It is also generally true that the mean lower layer depth at the sill is less than the mean upper layer depth, and thus solutions such as shown in Figure 5.3.1b are ruled out. The maximal value of $Q/w$ (Figure 5.7.8) decreases as the strength of rotation (the value of $w$) increases, provided that $w$ is less than about 1.6. However this trend is reversed at higher values of $w$, corresponding to the transition between singly separated sill flow (dots) and doubly separated sill flow (crosses). The increase in the exchange transport with increasing rotation contrasts with the usual tendency in single-layer hydraulics for the flux to decrease with rotation.[1] The new trend is due in part to the zero potential vorticity model, which has no constraining boundary layer structure. In addition, the tendency for rotation to squash a separated layer against its right-hand wall has different consequences in single- and two-layer flows. In the former, the effect is to constrict the cross-section of the layer and thereby diminish the transport. In the two-layer setting, the squashing of one layer against a wall relieves the other layer. For comparison, the flux predicted by the Whitehead et al. (1974) model for symmetrical upper and lower layers (Equations 5.7.21, 22) is indicated by a dashed line in Figure 5.7.8. The values overestimate the maximal exchange values at low and moderate rotation, but

Laboratory and numerical experiments (e.g. Whitehead and Miller 1979, Dalziel 1988, Whitehead and Hunkins 1992, and Rabe, et al. 2007) with two-layer, rotating exchange flows have so far failed to reproduce double separation of the interface. Where double separation is predicted ($w >$ about 1.5) the flow is instead observed to become unstable. The result is a time-dependent flow field marked by the presence of eddies and with mean features quite different from that predicted by the zero potential vorticity theory. These complications may well prevent the increase in flux past $w$=1.5 that is predicted in Figure 5.7.8. The increase in maximal flux predicted beyond $w$=1.5 has not been reproduced.

[1] The trend for the maximal flux to increase when $w$ exceeds 1-2 deformation radii is also predicted in the Reimenschneider et al. 2005 model.

Is it possible to relate $Q$ to some well-defined and easily measured property of the flow in the upstream basin? To investigate this question further it will be helpful to have a better understanding of the behavior of the upper layer in the basin. Any mouth state can be formally extended into the basin by allowing the width $w_B$ to gradually increase from its value $w$ at the mouth and requiring that $Q$ and $\Delta B$ be conserved. In all cases, the upper layer will separate at sufficiently large $w_B$ if it is not already separated at the mouth. Once separated, the flow will continue, unaltered, into the basin until some other process intervenes. The velocity and depth profiles of the separated upper layer are given by (5.7.30) and (5.7.31). As explained in Section 2.3, the criticality of the flow may be identified by the presence or lack of velocity reversals. If the upper layer depth decreases monotonically away from the left wall (Figure 5.7.9a), so that $v_1$ is everywhere <0, then the flow is supercritical. The presence of a depth maximum and a corresponding velocity reversal (Figure 5.7.9c) implies subcritical flow. In this case there will be a band of reverse flow along the left wall carrying fluid towards the mouth. If the maximum depth occurs at the wall (Figure 5.7.9b) then $v_1$ is zero there and the flow is critical.

If one begins by selecting a sill flow that is submaximal, then for that $Q$ and $w$ there are two possible mouth states, one supercritical and one subcritical. The usual stability considerations require that we select the subcritical root. This mouth state may be separated or non-separated; in the latter case separation will occur within the wide basin. An example based on the case $w$=0.5 (Figure 5.7.10a) shows an attached mouth flow that becomes separated in the basin. The anticipated band of counterflow is present along the wall. For the maximal state the mouth flow is critical. Stability considerations now require a transition to supercritical flow as the basin is approached (Figure 5.7.10b). The separated upstream state is distinguished from the submaximal case in that the current is narrower and contains no velocity reversals. Of course, the supercritical flow could pass through a hydraulic jump and lose these distinguishing characteristics.

The separated upstream width $w_e$ is a clearly defined property of the basin flow and, as such, is a potentially convenient property on which to base a weir relation. An implicit weir formula for the case of attached sill flow can be developed by equating $\Delta B$ at the sill (see 5.7.15 with $d$=1 and $h$=$z_I$-1) with (5.7.33). With the help of (5.7.34) this equality can be written as

$$\left( \frac{w_e}{2} + \frac{(2Q)^{1/2}}{w_e} \right)^2 = 2 - 2\bar{d}_{2c} - \frac{Q^2\left(1-2\bar{d}_{2c}\right)}{w^2(\bar{d}_{2c}(1-\bar{d}_{2c}) - w^2/12)^2}, \quad (5.7.35)$$

where $\bar{d}_{2c}$ is determined by (5.7.16) as applied at the sill:

$$\frac{Q^2}{w^2} = \frac{\left(\bar{d}_{2c}\left(1-\bar{d}_{2c}\right) - w^2/12\right)^3}{\left(\bar{d}_{2c}\left(1-\bar{d}_{2c}\right) - w^2/12 + \left(1-2\bar{d}_{2c}\right)^2\right)}. \quad (5.7.36)$$

Together, (5.7.35) and (5.4.34) provide a relationship between $Q/w$, $w$, and $w_e$. Satellite or aircraft measurements of separated current width $w_e$ might thereby provide an estimate of the flux, provide that the width is clearly defined.

*d. The Strait of Gibraltar revisited.*

Conventional wisdom dictates that rotation is not a major influence in dynamically narrow straits such as Gibraltar and the Bab al Mandab. In the case of Gibraltar (Figure 5.6.1) the value of $(g'D_s)^{1/2}/f$ based on the average sill depth $D_s$=200m, and $g'$=0.02$ms^{-2}$ is 23$km$, which is significantly greater than the width $w^*\cong$13$km$ at Terifa Narrows. However, this gross estimate fails to account for the behavior of the upper layer at the eastern end of the strait, where it shallows and accelerates. Acoustic images and CTD sections have shown that this layer can separate from the northern coast at some point between Tarifa and Gibraltar. Corroboration of this phenomenon can be found in photographs of the strait from space (e.g. Figure 5.7.11), which suggest detachment of the (lighter) surface layer and outcropping of the (darker) lower layer near the northeastern corner of the strait.

We have already documented the tendency of maximal flows to produce an upstream separated width $w_e$ that is significantly smaller than that for submaximal flow. The observed separation width ($w_e^*$=15±1$km$) is therefore a potential discriminator. Although the idealized theory does not account for barotropic flow, nor for the geometric complexities of the Strait, it is still instructive to compare the predicted maximal and submaximal values of $w_e$ with observations. To do so, fix the width of the idealized, constant width channel as $w$=.57, which corresponds to the above estimate $w^*f/(g'D_s)^{1/2}$=13/23. As shown by Timmermans and Pratt (2005) the corresponding $w_e^*$ for maximal flow is 15$km$, within the range of uncertainty of the observed value, whereas submaximal solutions would have $w_e^*$>32km. The predicted volume flux for the maximal case is $Q^*$=0.92±0.03, which lies at the upper end of the estimate 0.78±0.17 for the upper layer flux obtained by Tsimplis and Bryden (2000). A number of refinements are called for here, but the results suggest that the flow was maximal at the time of the observations.

**Exercises**

1) Show that the 'zero potential vorticity' limit $D_s<<D_{i\infty}$ is equivalent to the limit in which the global Rossby deformation radius (5.1.12) is large compared to the 'local' deformation radius $(g'D_s)^{1/2}/f$.

2) *Barotropic 'similarity' solution for flow through a pure contraction.*

Suppose that for two-layer, zero potential vorticity flow, the layer fluxes $Q_1$ and $Q_2$, both >0, are specified. Then show that equation (5.7.15) admits a barotropic solution

for which the interface is horizontal ( $\overline{v}_1 = \overline{v}_2$ ) and the layer depths are constant in *x* and *y*. Show that the values of $\overline{v}_1$ , $\overline{v}_2$ , and the layer depths are determined from

$$\overline{v}_1(y) = \overline{v}_2(y) = \frac{Q_1 + Q_2}{w(y)d} \text{ and } \quad d_2 = d - d_1 = \overline{d}_2 = \frac{Q_2 d}{Q_1 + Q_2}.$$

Show that the Bernoulli function $\Delta B$ is not a free parameter for this solutions but instead is determined from as $h+d_2$.

3) *Critical conditions for singly-detached sill flow.*

(a) Consider a singly-detached exchange flow where the interface between the two layers intersects either $z = z_T$ or $z = 0$. For a positive interface slope $\left(\overline{v}_2 - \overline{v}_1 \geq 0\right)$, show that the flow detaches from the right wall ($x = w/2$) when

$$\overline{d}_2 \geq d - \left(\overline{v}_2 - \overline{v}_1\right)\frac{w}{2},$$

and that it detaches from the left wall ($x = -w/2$) when

$$\overline{d}_2 \leq \left(\overline{v}_2 - \overline{v}_1\right)\frac{w}{2}.$$

(b) With the origin $x=0$ positioned as the left wall (as in Figure 5.7.2b), show that the velocity and depth profiles for the case of lower layer separation are given by

$$\overline{v}_i(x,y) = w - w_s - x + \hat{v}(y)$$

$$d_1(x,y) = \begin{Bmatrix} d(y) - \hat{v}_-(x + w_s - w) & (x \geq w - w_s) \\ d(y) & (x < w - w_s) \end{Bmatrix} \qquad (5.7.35)$$

and

$$d_2(x,y) = \begin{Bmatrix} \hat{v}_-(x + w_s - w) & (x \geq w - w_s) \\ 0 & (x < w - w_s) \end{Bmatrix}$$

where the ˆ over a variable implies its value at $x = w - w_s$, the point where the interface intersects the bottom of the channel $z = 0$, and $\hat{v}\pm = \hat{v}_2 \pm \hat{v}_1$.

(c) Show that the volume fluxes in the two layers are given by

$$Q_2 = w_s^2(\hat{v}_2 - \hat{v}_1)\left(\frac{\hat{v}_2}{2} - \frac{w_s}{3}\right) \qquad (5.7.36)$$

and

$$Q_1 = dw\left(\hat{v}_1 - w_s + \frac{w}{2}\right) - w_s^2(\hat{v}_2 - \hat{v}_1)\left(\frac{\hat{v}_1}{2} - \frac{w_s}{3}\right). \qquad (5.7.37)$$

(d) By evaluating the Bernoulli function where the interface intersects the bottom, show that

$$\Delta B = \frac{\hat{v}_+\hat{v}_-}{2} + z_T - d\,, \qquad (5.7.38)$$

where $\hat{v}_\pm = \hat{v}_2 \pm \hat{v}_1$. Assuming the net transport to be zero ($Q = -Q_1 = Q_2 > 0$), show that (5.7.36), (5.7.37), and (5.7.38) can be written as

$$G_1\left(\hat{v}_-, \hat{v}_+, w_s; d, w\right) = w_s^2\hat{v}_-^2 - dw(\hat{v}_- - \hat{v}_+ - w + 2w_s) = 0\,, \qquad (5.7.39)$$

$$G_2\left(\hat{v}_-, \hat{v}_+, w_s\right) = w_s^2\hat{v}_-\left(\frac{\hat{v}_+ + \hat{v}_-}{4} - \frac{w_s}{3}\right) - Q = 0\,, \qquad (5.7.40)$$

and

$$G_3\left(\hat{v}_-, \hat{v}_+; d\right) = \hat{v}_+\hat{v}_- - 2\left(\Delta B - z_T + d\right) = 0\,. \qquad (5.7.41)$$

(e) By interpreting (5.7.39-41) as three functions in the three variables $\hat{v}_-$, $\hat{v}_+$ and $w_s$, show that the critical conditions is.

$$\hat{v}_- w_s\left\{wd\left(3\hat{v}_+^2 - 6\hat{v}_+ w_s + 4w_s^2\right) - 6\hat{\upsilon}_- wd\left(-\hat{v}_+ + 2w_s\right)\right.$$

$$+\hat{v}_-^2\left(3wd + 2w_s^2\left(-3\hat{v}_+ + 4w_s\right)\right)\Big\} = 0\,. \qquad (5.7.42)$$

4. Show that a symmetric state of marginal separation, in which the interface contacts the upper right and lower left corners, occurs when $d = (\overline{v}_2 - \overline{v}_1)w$ and $\overline{v}_2 = -\overline{v}_1$. Show using (5.7.17) that this state is critical when $d=w^2$.

5. *Characteristic speeds under conditions of attachment*. By observing that the profiles (5.7.5-5.7.7) are valid for time-dependent flow, show that the equation for conservation of $y$-momentum is given by

$$\frac{\partial \hat{v}}{\partial t} + \left[\hat{v}\left(1 - \frac{2\overline{d}_2}{d}\right) + v_b\right]\frac{\partial \hat{v}}{\partial y} + \left(1 - \frac{\hat{v}^2}{d}\right)\frac{\partial \overline{d}_2}{\partial y} = 0\,,$$

where $\hat{v} = \overline{v}_2 - \overline{v}_1$ denotes the shear velocity and $v_b = (\overline{v}_1\overline{d}_1 + \overline{v}_2\overline{d}_2)/d$ denotes the (constant) barotropic velocity. Further show that the continuity equation for either of the layers may be written as

$$\frac{\partial \overline{d}_2}{\partial t} + \left[(d - \overline{d}_2)\frac{\overline{d}_2}{d} + \frac{w^2}{12}\right]\frac{\partial \hat{v}}{\partial y} + \left[\hat{v}(1 - \frac{2\overline{d}_2}{d}) + v_b\right]\frac{\partial \overline{d}_2}{\partial y} = 0\,.$$

From these two expression deduce the characteristic speeds $c_\pm$ and show that they can put in the simplified form given by the equation following (5.7.17).

6. Consider a configuration in which the interface of the two-layer, zero potential vorticity exchange flow (with zero net exchange) contacts both the upper right and lower left corners of the channel. Show that such a flow can be critical only for $w=d^{1/2}$ or $w=(3d)^{1/2}$.

**Figure Captions**

Figure 5.7.1. Initial condition for the lock exchange problem (a). Plan view of the basin and strait geometry (b). (From Timmermans and Pratt, 2005)

Figure 5.7.2. Definition sketches for the flow cross section (a) and the various possible separation states with a positive interface tilt (b-d). (From Timmermans and Pratt, 2005)

Figure 5.7.3. The nondimensional exchange transport per unit width as a function of the mean lower layer depth. The flow is assumed to occur at the sill section ($d$=1) and is critical and attached to both sidewalls. Gaps in the curve for $w$=0.87 correspond to separated flow, for which Figure 5.7.4 should be consulted. The dots and crosses indicate

maximal exchange values calculated under two different assumptions as described in the text. (From Timmermans and Pratt, 2005)

Figure 5.7.4. The flow rate per unit width as a function of the separated width of the current at the sill ($w_s/w$ for single detachment and $w_b/w$ for double detachment) for various $w$. By symmetry, $w_s$ may be interpreted as the lower layer width for lower layer detachment, or the upper layer width for upper layer detachment. (From Timmermans and Pratt, 2005).

Figure 5.7.5. Pseudo Froude number plane for two-layer flow with background rotation, zero potential vorticity, and contained in a self-similar channel geometry: $w/d^2=1$. The inset shows the (dashed) critical curve and the (sold) boundaries demarking various regions of separation. The shaded region of the inset corresponds to subcritical flow. The layer Froude numbers are defined as $F_n = \overline{v}_n / d^{1/2}$, where $d$ is the total channel depth and $\overline{v}_n$ is the centerline velocity. If the layer in question is separated and does not exist at the channel centerline, $\overline{v}_n$ is defined by formally extending the velocity profile for that layer to the centerline. The solid curves in the main part of the diagram are of constant $Q^{1/2} / (\Delta B - z_T)$, while the dashed curves are of constant $Q/d^2$. To present too much clutter, the contours on the dashed lines are not labeled. However, the value of $Q/d^2$ increases as one moves away from the origin, corresponding to shallower depths. Solutions are traced along solid lines. Stars indicate sill controls while the square indicates a virtual control. (A rotated version of Figure 5.7.9 from Reimenschneider et al. 2005.)

Figure 5.7.6. An example of submaximal flow based on the $Q^{1/2} / (\Delta B - z_T) = -1.4$ contour of Figure 5.7.5. The top three panels show $d_2$, $v_2$, $v_1$, respectively. The dashed curves in the middle two figures show where the edge of the layer in question contacts the bottom or top lid. The bottom panel is a side view showing the intersection of the interface with the left wall (dashed-dotted curve) and the right wall (dashed curve.) (Constructed from Reimenschneider et al. 2005, Figure 12.)

Figure 5.7.7. Cross sections of maximal exchange configurations at the sill, mouth and in the upstream basin. (From Timmermans and Pratt, 2005 Fig. 17)

Figure 5.7.8. The nondimensional maximal volume flux per unit width $Q_{max}/w$ ($=Q^*_{max}/w^*g'^{1/2}D_s^{1/2}$) for pure exchange flow. The geometry is shown in Figure 5.7.1 and the lower layer is assumed to be inactive in its deep upstream basin. The ×, • and + correspond to attached, singly-separated, and doubly separated sill flow, as showing by the insets. The dashed curve indicates the $Q/w$ as given by the Whitehead et al. (1974) formula (5.7.21) for attached flow with symmetric upper and lower layers. The connecting dashed line gives the value $Q/w=1/6$ given by the same authors for symmetrical, detached flow, assuming that regions occupied by only one of the layers are quiescent. (Based on Timmermans and Pratt, 2005, Figure 16.)

Figure 5.7.9. Cross section of the separated flow in the upstream basin (From Timmermans and Pratt, 2005, Figure 5.7.7.)

Figure 5.7.10. Plan views of the flow upstream of the sill. The upper layer velocity and depth profiles are shown at the mouth (or entrance) of the strait and in the upstream basin after detachment has occurred. In both cases the sill width $w$ and mouth width $w_m$ are 0.5. Frame (a) shows a submaximal case with subcritical flow at the mouth and in the basin. Frame (b) shows the maximal flow with critical flow at the mouth and supercritical flow in the basin (From Fig. 10 of Timmermans and Pratt, 2005.)

Figure 5.7.11. October 1984 space shuttle photograph of the Strait showing a (dark) area thought to be the lower layer outcrop south of Gibraltar. The strait width at the narrowest section is about 13 *km*, while that at the separation point is 15±1 *km*. (NASA, LBJ Space Center Photo S-17-34-080.)

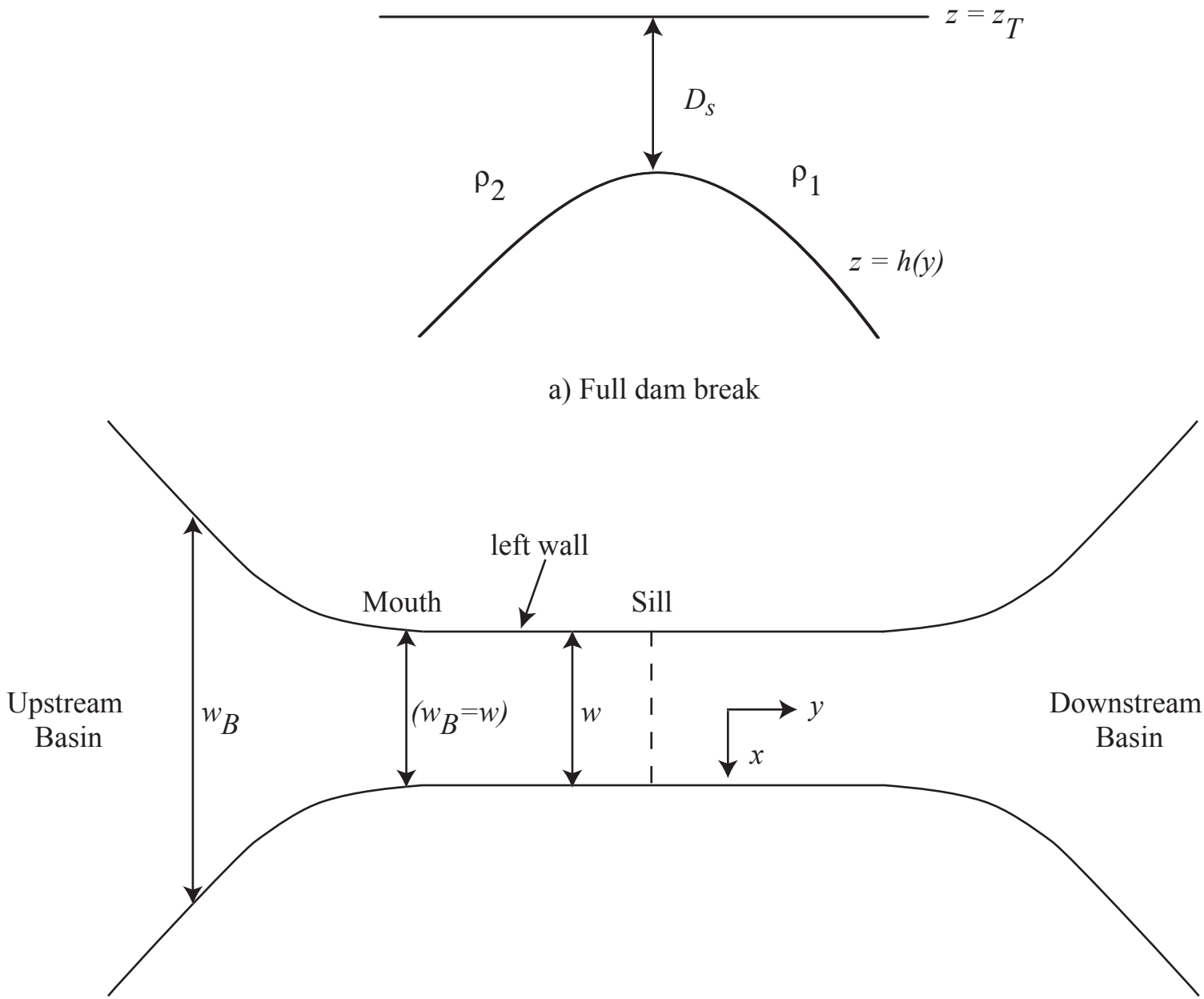


a) Full dam break

b) Plan view

Fig 5.7.1

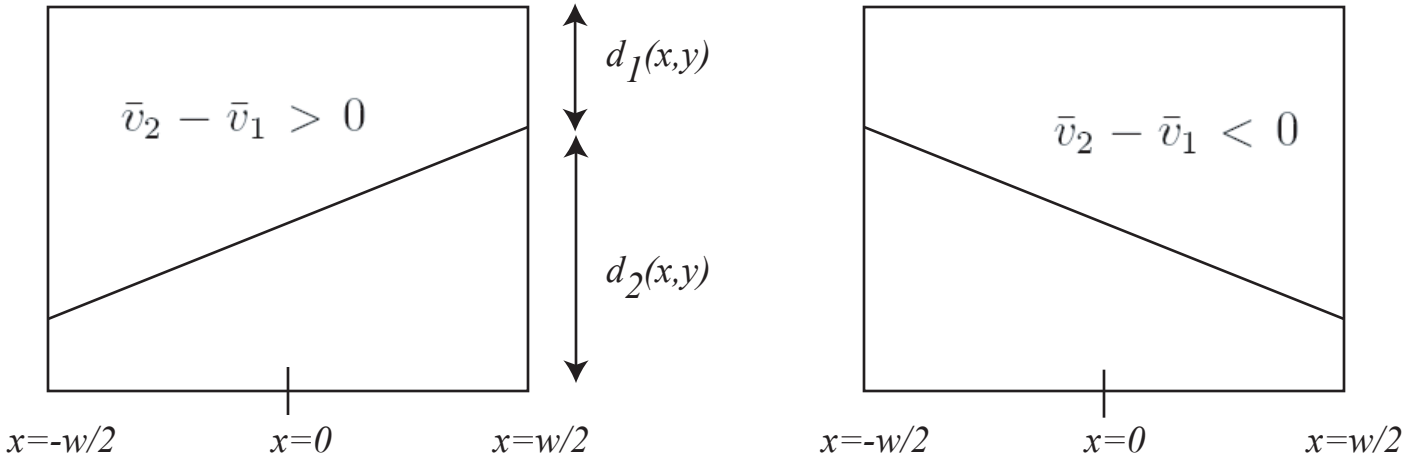


a) Attached flows

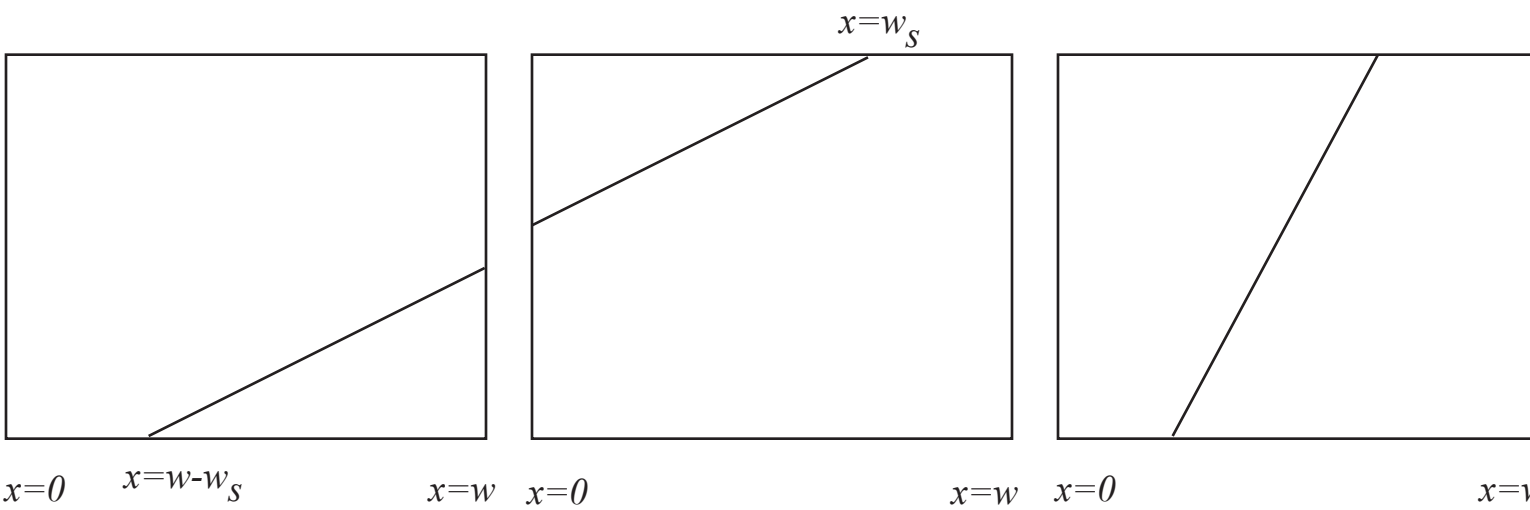


b) Singly-detached 1

c) Singly-detached 2

d) Doubly-detached

Fig 5.7.2

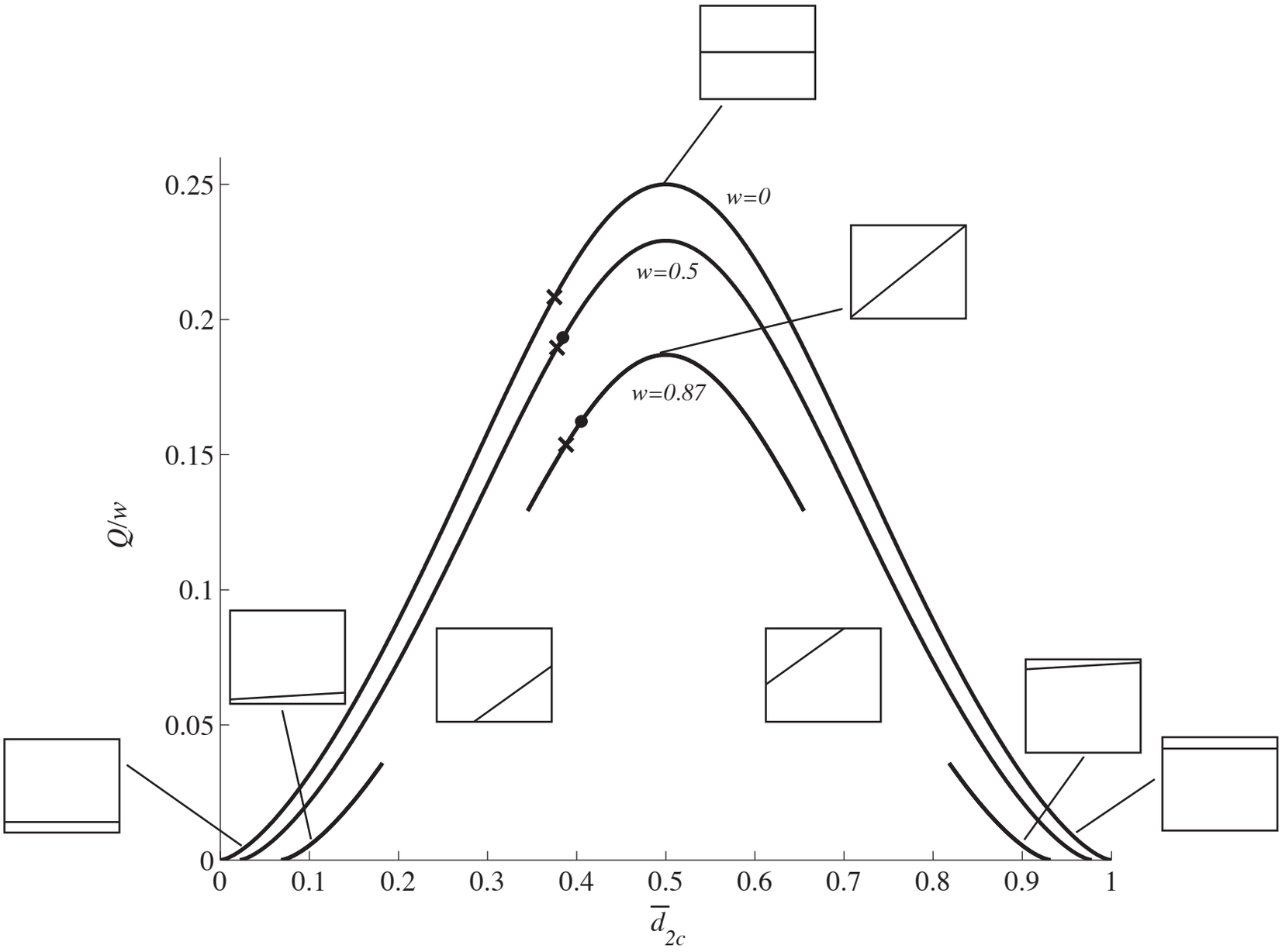
0.25
0.2
0.15
0.1
0.05
0
Q/w
w=0
w=0.5
w=0.87
0
0.1
0.2
0.3
0.4
0.5
0.6
0.7
0.8
0.9
1
$\overline{d}_{2c}$

Fig 5.7.3

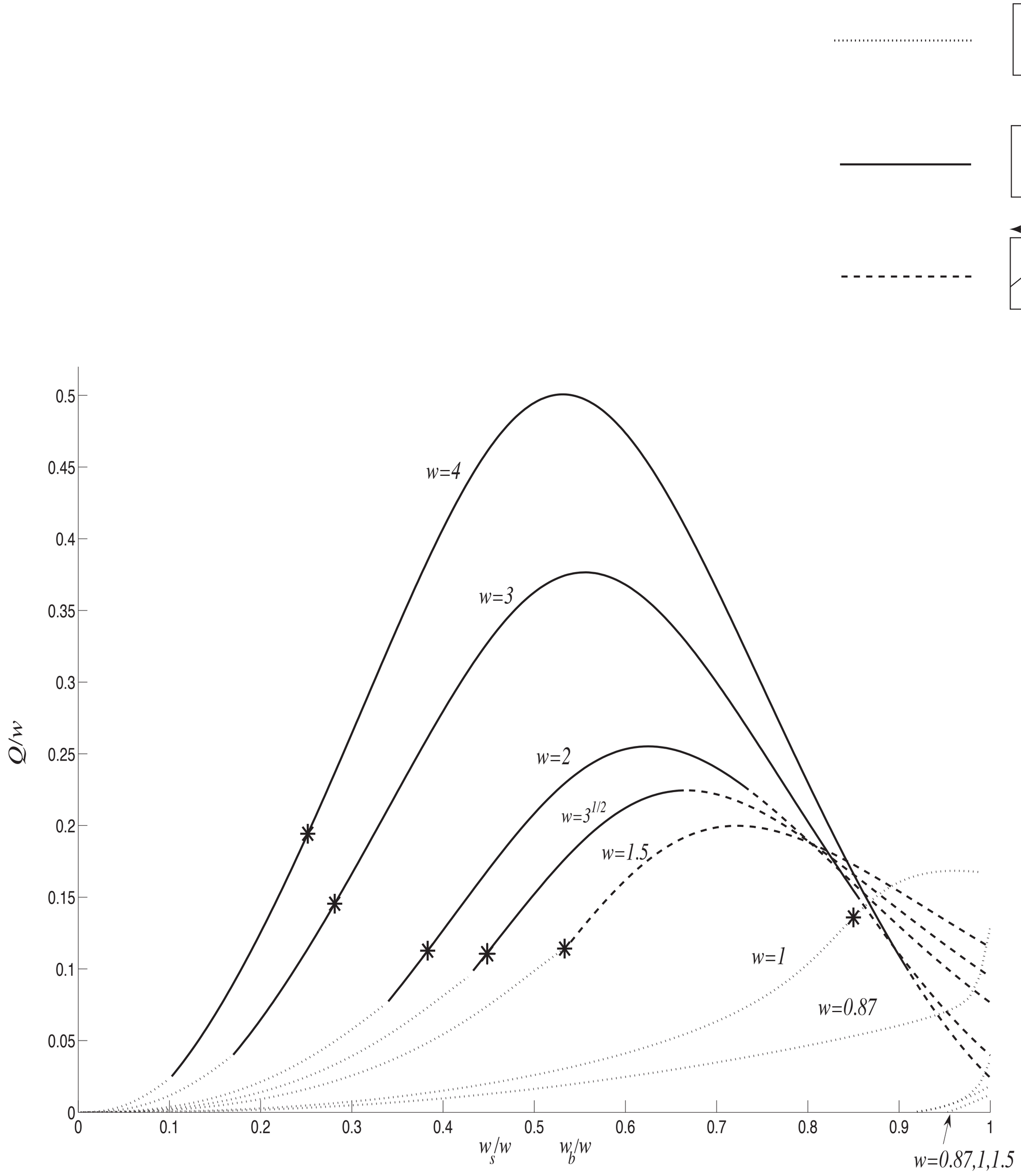
$w_s$
$w_b$
$w_s$
0.5
0.45
0.4
0.35
0.3
0.25
0.2
0.15
0.1
0.05
0
Q/w
w=4
w=3
w=2
w=3^1/2
w=1.5
w=1
w=0.87
0
0.1
0.2
0.3
0.4
0.5
0.6
0.7
0.8
0.9
1
w_s/w
w_b/w
w=0.87,1,1.5

Figure 5.7.4

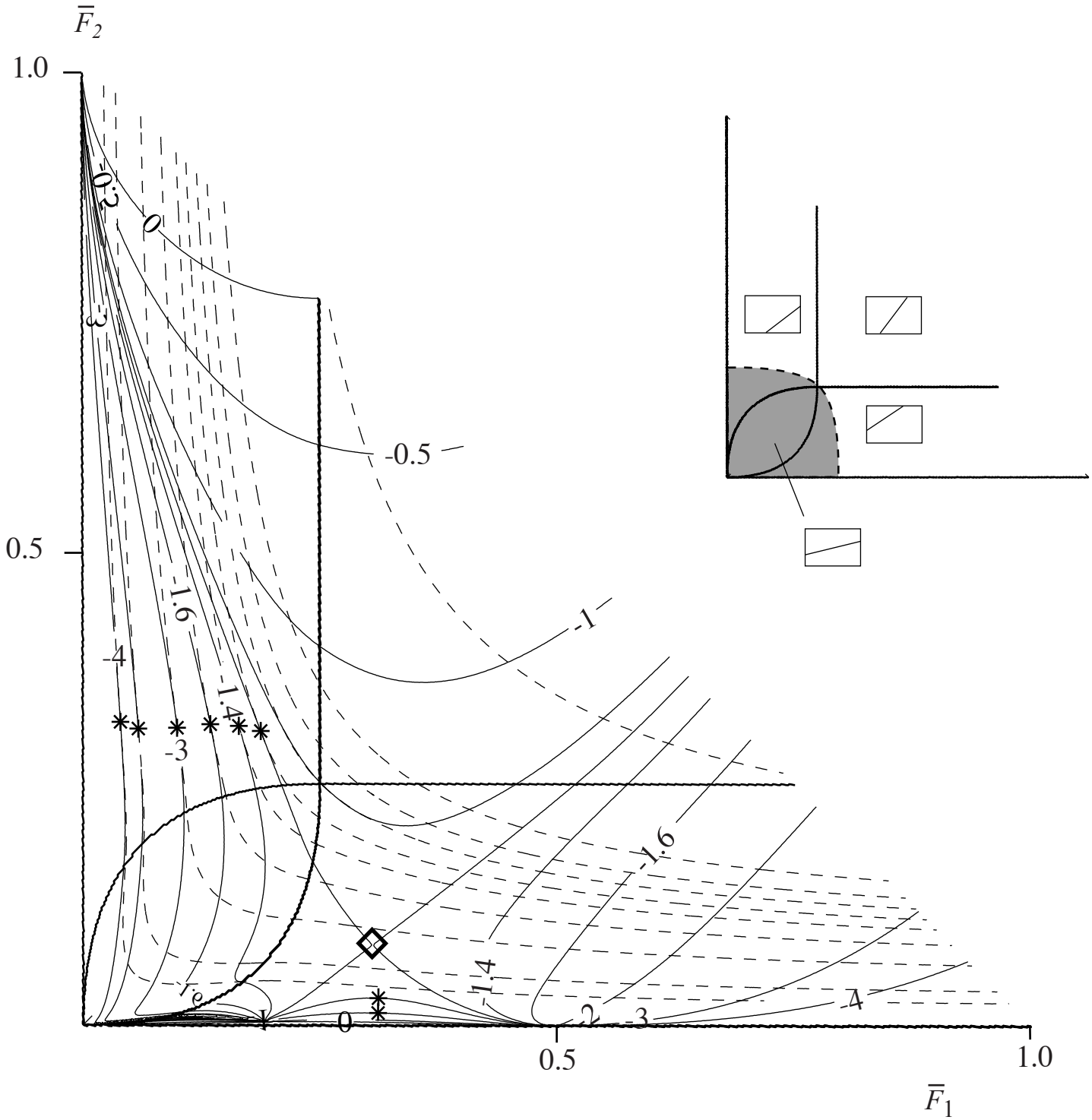
$\overline{F}_2$
1.0
0.5
-0.2
0
-3
-0.5
-1
-1.6
-4
-1.4
-3
-1.6
-1.4
$r_e$
1
0
2
-3
-4
0.5
1.0
$\overline{F}_1$

Fig. 5.7.5

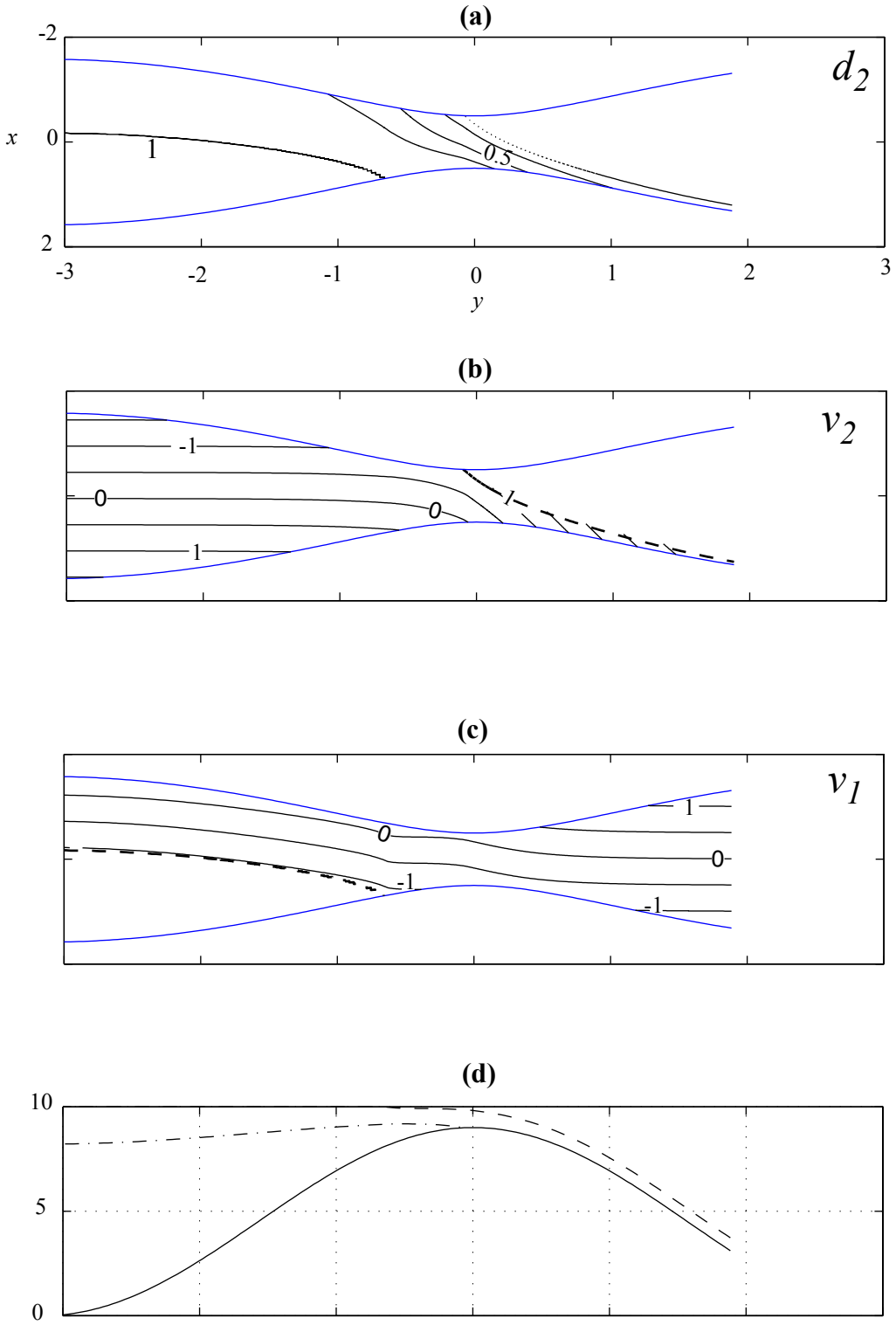


Figure 5.7.6

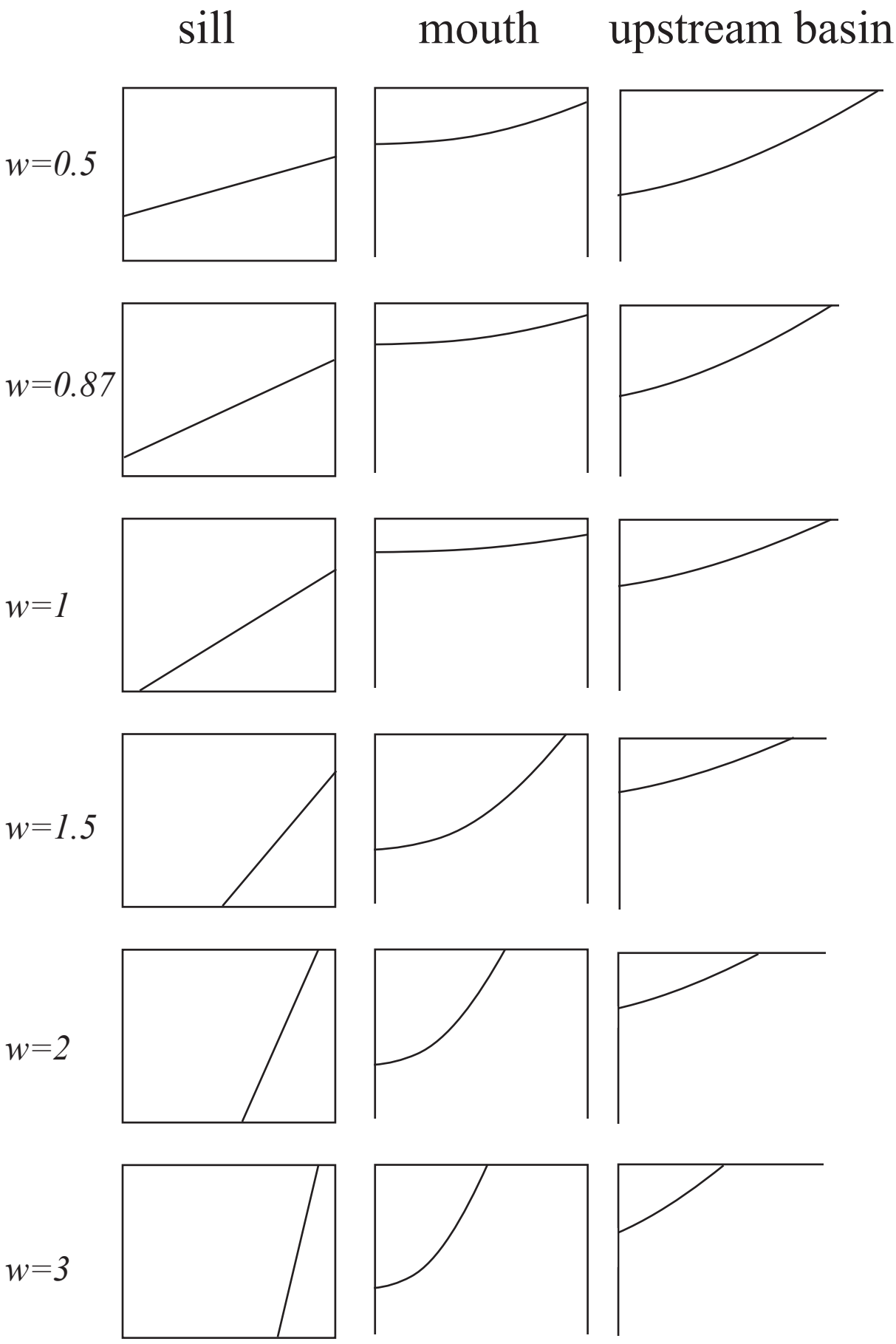


Fig 5.7.7

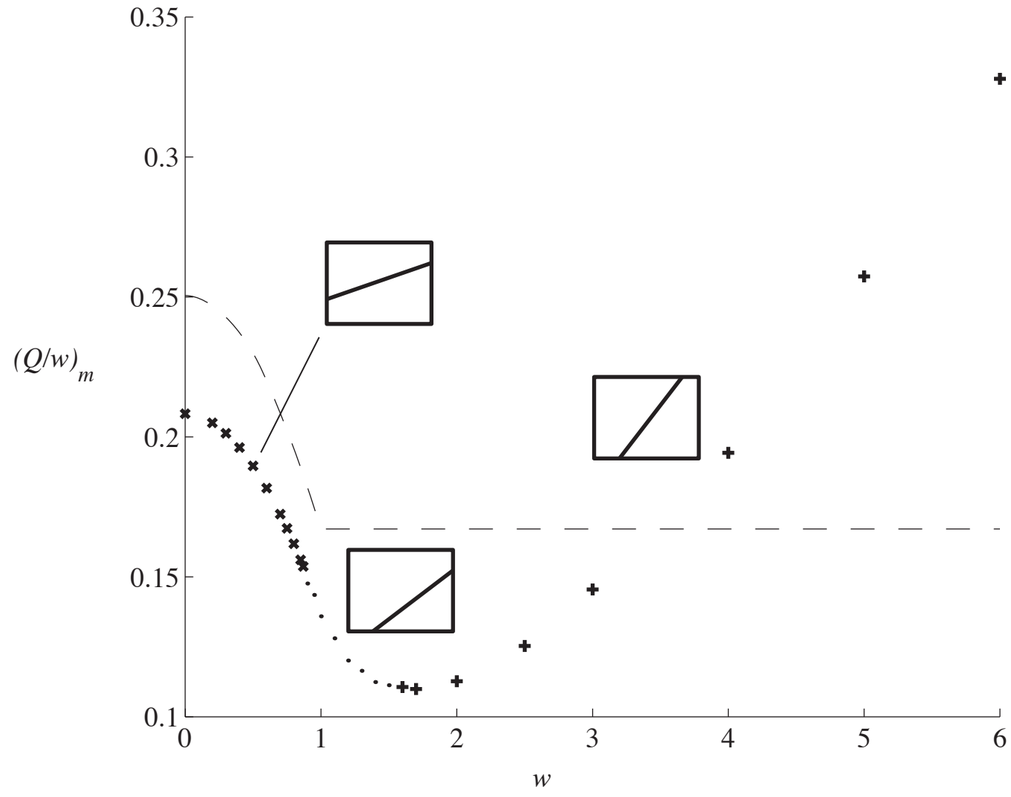


Figure 5.7.8

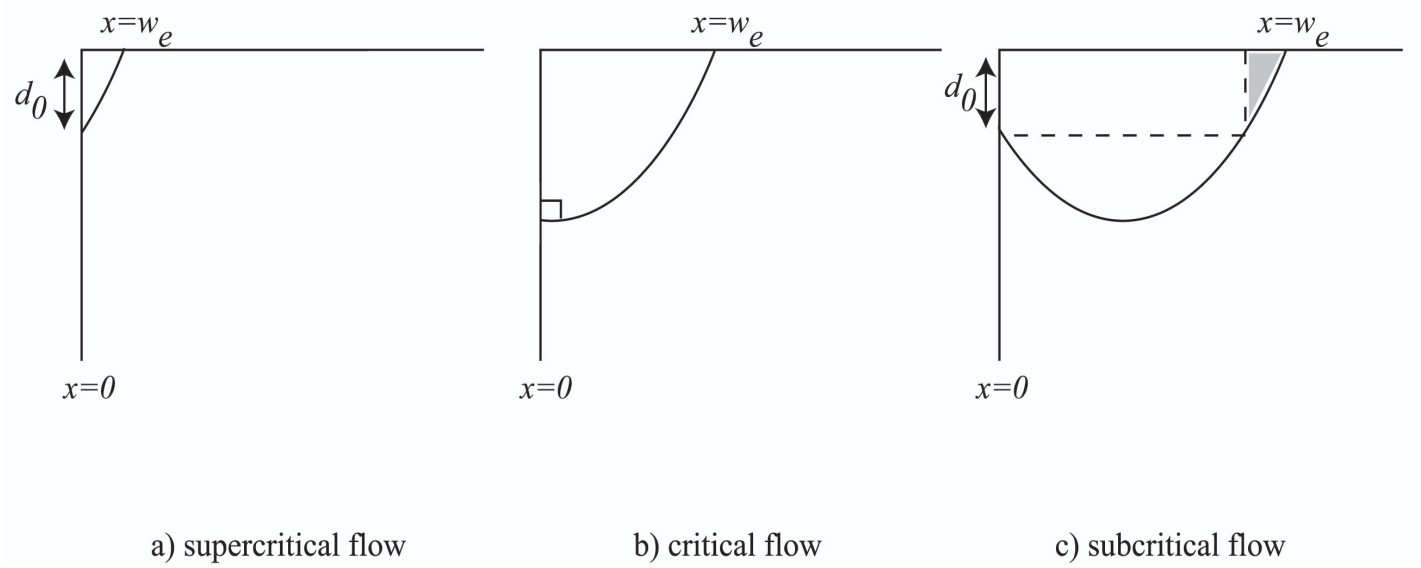


a) supercritical flow b) critical flow c) subcritical flow

Figure 5.7.9

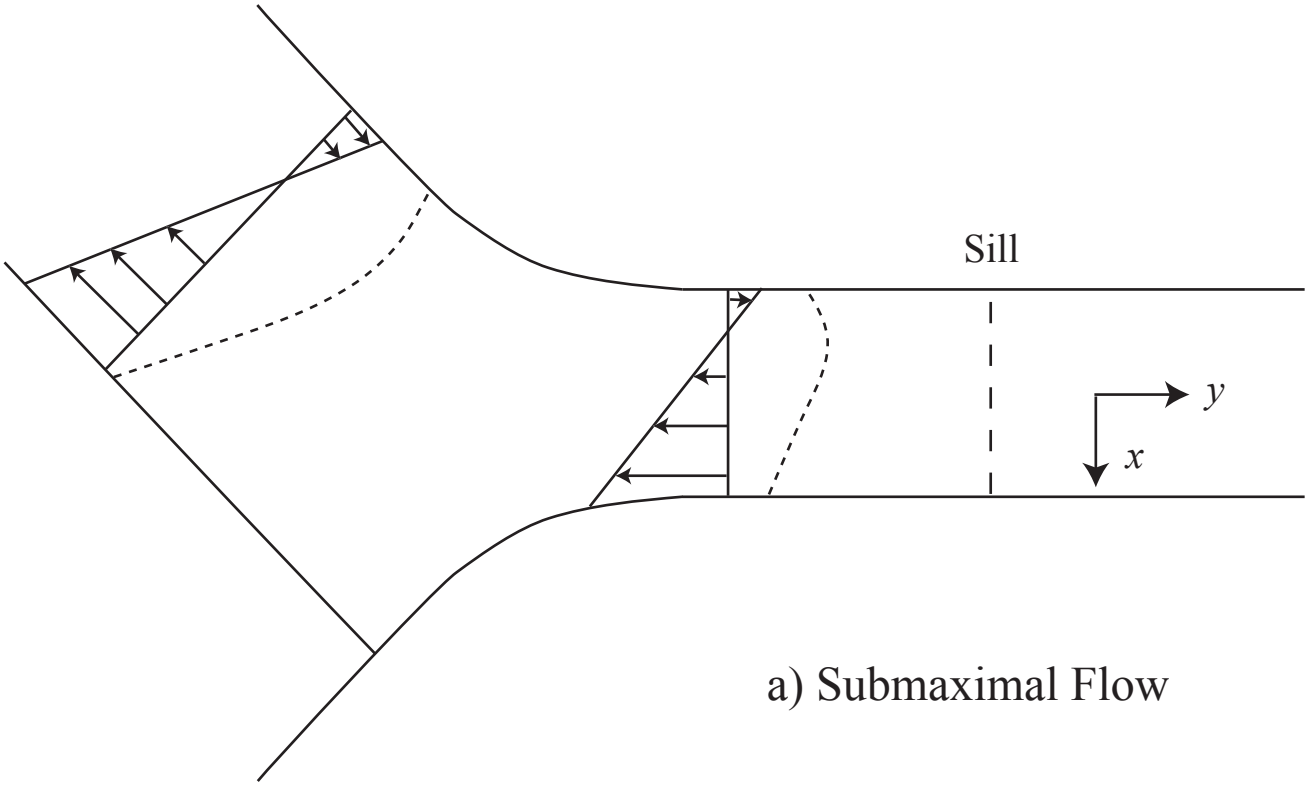


a) Submaximal Flow

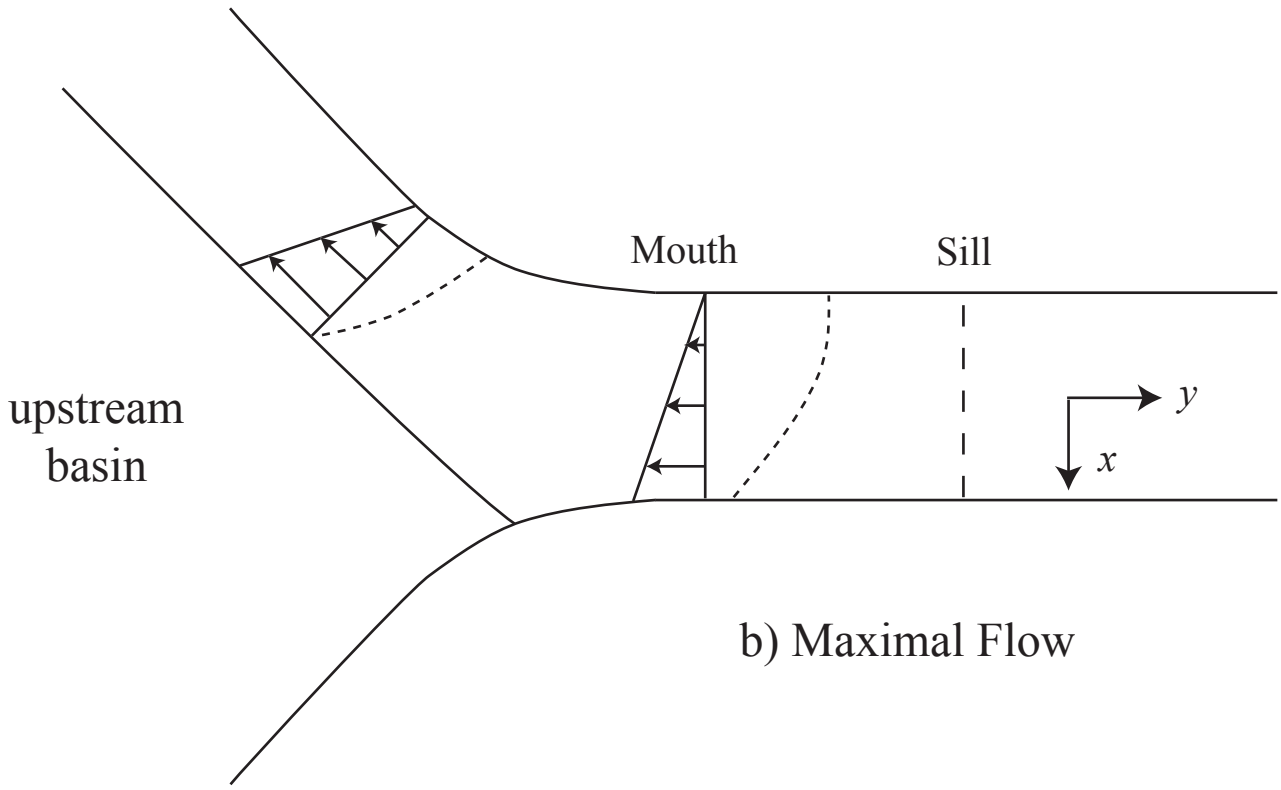


b) Maximal Flow

Figure 5.7.10

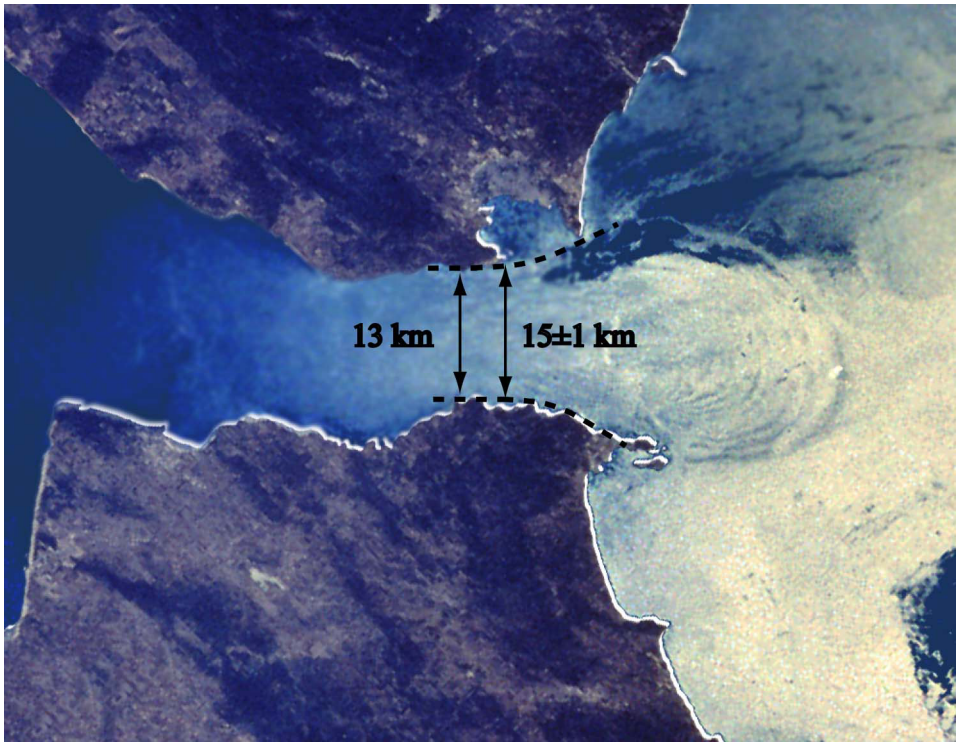


Figure 5.7.11